Tectonics

RESEARCH ARTICLE
10.1029/2017TC004896

Special Section:
Geodynamics, Crustal and Lithospheric Tectonics, and active deformation in the Mediterranean Regions (A tribute to Prof. Renato Funiciello)

Opposite Subduction Polarity in Adjacent Plate Segments

Mireia Peral[1], Ágnes Király[2,3], Sergio Zlotnik[4,5], Francesca Funiciello[2], Manel Fernàndez[1], Claudio Faccenna[2], and Jaume Vergés[1]

[1]Group of Dynamics of the Lithosphere, Institut de Ciències de la Terra Jaume Almera (ICTJA-CSIC), Barcelona, Spain, [2]Laboratory of Experimental Tectonics, Department of Sciences, Università degli Studi Roma Tre, Rome, Italy, [3]The Centre for Earth Evolution and Dynamics, University of Oslo, Oslo, Norway, [4]Department of Civil and Environmental Engineering, Universitat Politècnica de Catalunya, Barcelona, Spain, [5]School of Ocean and Earth Sciences, Tongji University, Shanghai, China

Key Points:
- Mantle flow induced by opposed adjacent plates is asymmetrical showing a progressive merging of the toroidal cells when trenches approach
- Trench retreat velocities are not steady and increase/decrease while trenches approach/separate
- The first-order consequences of the dynamics of double subduction systems are relevant in natural scenarios

Correspondence to:
M. Peral,
mperal@ictja.csic.es

Citation:
Peral, M., Király, Á., Zlotnik, S., Funiciello, F., Fernàndez, M., Faccenna, C., & Vergés, J. (2018). Opposite subduction polarity in adjacent plate segments. *Tectonics*, *37*. https://doi.org/10.1029/2017TC004896

Received 14 NOV 2017
Accepted 4 SEP 2018
Accepted article online 6 SEP 2018

Abstract Active and fossil subduction systems consisting of two adjacent plates with opposite retreating directions occur in several areas on Earth, as the Mediterranean or Western Pacific. The goal of this work is to better understand the first-order plate dynamics of these systems using the results of experimental models. The laboratory model is composed of two separate plates made of silicon putty representing the lithosphere, on top of a tank filled with glucose syrup representing the mantle. The set of experiments is designed to test the influence of the width of plates and the initial separation between them on the resulting trench velocities, deformation of plates, and mantle flow. Results show that the mantle flow induced by both plates is asymmetric relative to the axis of each plate causing a progressive merging of the toroidal cells that prevents a steady state phase of the subduction process and generates a net outward drag perpendicular to the plates. Trench velocities increase when trenches approach each other and decrease when they separate after their intersection. The trench curvature of both plates increases linearly with time during the entire evolution of the process regardless their width and initial separation. The interaction between the return flows associated with each retreating plate, particularly in the interplate region, is stronger for near plate configurations and correlates with variations of rollback velocities. We propose that the inferred first-order dynamics of the presented analog models can provide relevant clues to understand natural complex subduction systems.

1. Introduction

The interaction of two subducting plates having opposite vergence has been recognized in several regions on Earth (Figure 1). A complex slab interaction occurs beneath Taiwan due to the presence of two opposite subduction zones that intersect at a right angle (e.g., Lallemand et al., 2001; Lin & Kuo, 2016). Farther south, the Manila slab is dipping east, whereas in the south the Philippine slab dips west (e.g., Hall & Spakman, 2015). In New Zealand, the Australian plate is being subducted beneath the Pacific plate with opposite polarity to the subduction along the Hikurangi Margin (e.g., Lamb, 2011). The updated hypocenter distribution in the Pamir-Hindu Kush region displays a sharp lateral change in the dip of the Wadati-Benioff zone from the Hindu Kush, dipping to the north, to the Pamir arc, dipping to the southeast (Kufner et al., 2016; Liao et al., 2017). In Italy, some authors (e.g., Vignaroli et al., 2008) describe the Voltri Massif as an extensional domain formed as a consequence of a reversal subduction polarity at the junction between the Western Alps and the North Apennines. Tectonic reconstructions of the Alps-Carpathians-Dinarides system also show an opposed subduction polarity between the Alpine-Carpathian Front (S-dipping) and the Dinaric-Hellenic Front (NE dipping) since approximately 35 Ma (e.g., Handy et al., 2014). In the western Mediterranean Vergés and Fernàndez (2012) proposed the retreat of opposite subduction polarity in adjacent segments of the Ligurian-Tethys domain as the origin of the Alboran and Algerian back-arc basins and their respective orogenic systems.

Single-plate subduction systems and related dynamics have been extensively studied in the literature (e.g., Bellahsen et al., 2005; Garel et al., 2014; Ribe, 2010; Stegman et al., 2010). The velocity at which the subducting plate sinks into the underlying mantle depends on the balance between the driving and resisting forces. Kinematically, the subduction velocity v_s is determined by two main factors: (i) the plate advance velocity v_{sp} and (ii) the trench velocity v_t, such that $v_s = v_{sp} + v_t$ (e.g., Lallemand et al., 2008; Figure 2). Different modes of subduction are observed in nature depending on the relative velocity of the trench with respect to the plate (i.e., advancing/retreating trenches; e.g., Funiciello et al., 2008).

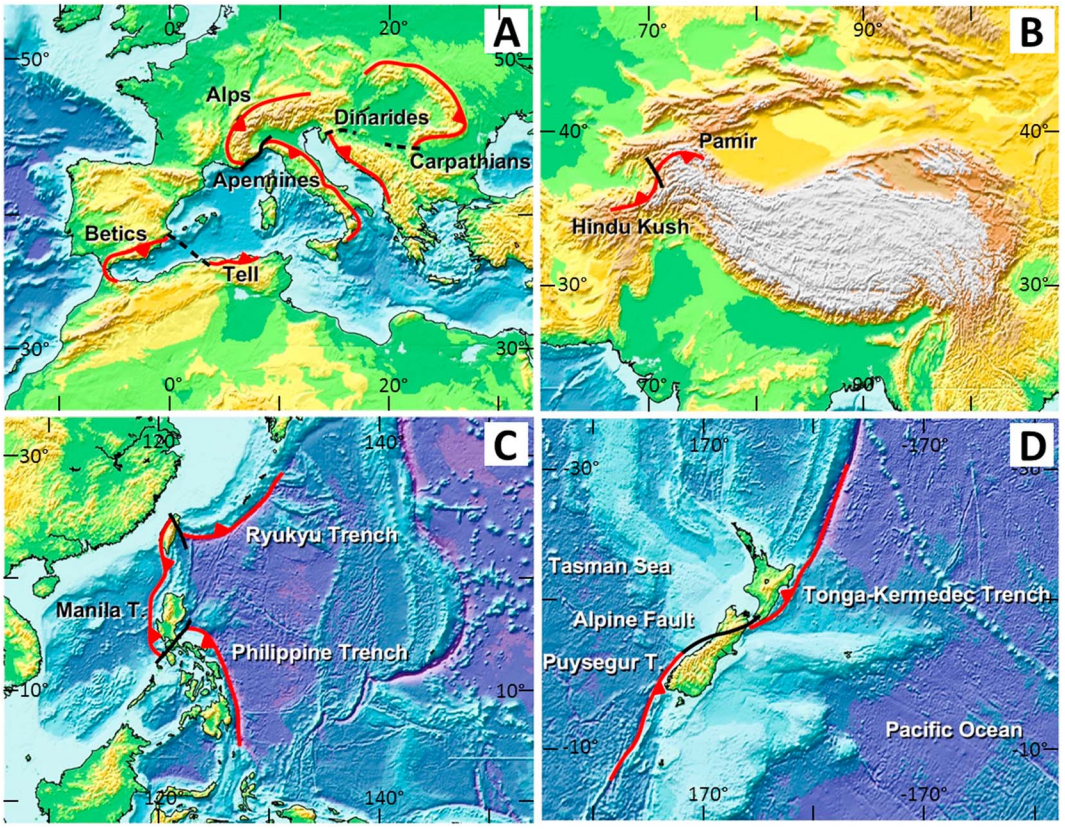

Figure 1. Location maps of double subduction systems with opposite polarity in adjacent segments. (a) Mediterranean region: Betic-Rif-Tell system (Vergés & Fernàndez, 2012); Alps-Apennines system (Vignaroli et al., 2008); Carpathians-Dinarides system (Handy et al., 2014). (b) West Tibet region: Pamir-Hindu Kush system (Kufner et al., 2016). (c) West Pacific region: Ryukyu-Manila system (Lallemand et al., 2001; Lin & Kuo, 2016); Manila-Philippine system (Hall & Spakman, 2015). (d) New Zealand region: Kermadec-Puysegur system (Lamb, 2011). The red lines and triangles denote trenches and subduction polarity; the continuous black lines denote active transform zones; the discontinuous black lines denote inactive transform zones.

Many numerical and analog models have been designed to address subduction-related mechanisms considering geological and geophysical observations. These models shed light on some characteristic processes occurring in subduction environments like hinge migration (e.g., Capitanio & Morra, 2012; Funiciello et al., 2004; Li & Ribe, 2012), plate bending (e.g., Capitanio et al., 2009; Conrad & Hager, 1999), or slab break-off

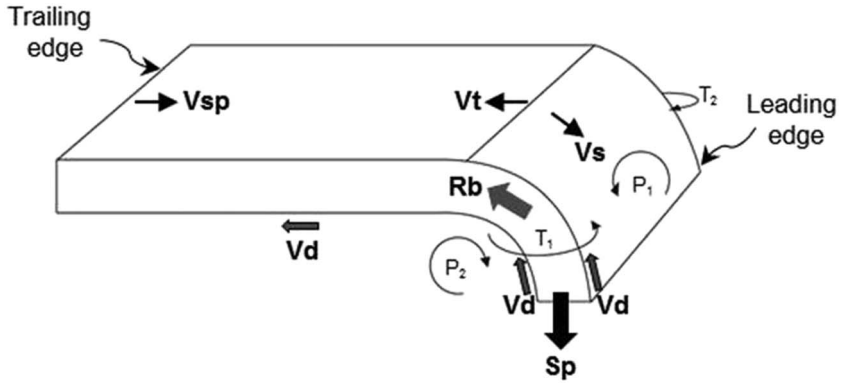

Figure 2. Scheme of the main forces active on the analog subduction models. Slab pull S_p is the driving force, while the plate bending R_b and the viscous shear V_d resist subduction. Kinematically, the subduction velocity v_s is defined as $v_s = v_{sp} + v_t$, where v_{sp} is the plate velocity and v_t is the trench velocity. In the setup of the analog experiments v_{sp} is forced to be zero by fixing the trailing edge of the plates and therefore $v_s = v_t$. P_1 and P_2 denote the poloidal components of the induced mantle flow, while T_1 and T_2 denote the toroidal components.

(e.g., Baumann et al., 2010; Magni et al., 2013). Other studies have focused on the influence of the overriding plate (e.g., Capitanio et al., 2011; Moresi et al., 2014), the rheological stratification of the slab and the upper-lower mantle (e.g., Funiciello et al., 2003), or the induced mantle flow (e.g., Funiciello et al., 2006; Király et al., 2017; Schellart, 2004; Stegman et al., 2006; Strak & Schellart, 2014).

It is known that the mantle flow induced by subduction rollback is divided into two principal components: poloidal and toroidal (Figure 2). The poloidal component acts in the mantle wedge and behind the slab, incorporating the flow in a vertical plane aligned with the subduction direction, while the toroidal component is a vortex-like flow displacing mantle around the slab edges. Evidence for poloidal/toroidal mantle flow is supplied by different geological, geophysical, and geochemical methods. Seismological and geodetic observations provide indirect constraints on short-term mantle circulations through present-day surface motions (e.g., Palano et al., 2017) and shear-wave splitting analysis (e.g., Díaz & Gallart, 2014; Long, 2016; Long & Silver, 2008). Magmatism and basalt geochemistry in terms of major and trace elements, as well as isotopic compositions, are also used to obtain information about mantle flow linked to subduction (Mullen & Weis, 2015).

Besides studies on single-plate subduction, the geodynamics of double subduction systems have received increasing attention in the last decade. Among others Mishin et al. (2008) and Čížková and Bina (2015) performed 2-D numerical models to analyze double subduction processes in which two plates are subducting simultaneously in the same direction. Di Leo et al. (2014) performed 3-D numerical models of a double-sided subduction case resembling the Molucca Sea subduction system in Eastern Indonesia. Holt et al. (2017) investigated the interaction between slabs with parallel trenches aligned in the same segment using 3-D numerical models. Recently, double subduction systems with parallel trenches and opposite polarity have been studied in a 3-D numerical modeling by Király et al. (2016). Their study focused on the interactions between the mantle flow cells induced by the retreating subduction trenches, distinguishing three phases in the evolution of the system. The first phase (phase 1) corresponds to the initial stage of subduction, during which the two slabs sink into the mantle until they reach the 660-km discontinuity. The initiation of the second phase (phase 2) coincides with the acceleration of slab rollback after the slabs interact with the upper-lower mantle boundary. After the trenches become aligned with each other, the progressive increase of the distance between trenches brings the third phase of the model (phase 3). The analysis of the stress propagation through the mantle varying the distance between plate edges from 2,000 to 62.5 km indicates that mantle flow interaction vanishes when plates are spaced more than ~600 km. In the model setup the authors assume perfect symmetry along the axis of the plates and periodic boundary conditions along the walls parallel with the trenches. Moreover, the size of the model domain remains the same for all experiments, such that the reduction of the separation between plates is accommodated by increasing the width of the plates. Although these conditions are adequate to study the stress propagation through the mantle, they impose some restrictions in analyzing the deformation of plates, the separate roles of the plate width and the initial separation between plates, and the geometry of the trench curvature.

In this work we present the results of analog models of double subduction systems with opposite polarity in adjacent plate segments varying the width of the plates and the initial separation between them. In contrast to the numerical study already presented by Király et al. (2016), aiming to be complementary, we focus on the deformation of plates and the variations of trench velocities rather than on the stress propagation within the sublithospheric mantle, covering a wide range of observed cases in nature. Specifically, the goals of the work are (1) to understand the first-order dynamics of the complex mantle flow generated in such subduction systems, (2) to analyze the interaction between the subducting plates in terms of their respective trench velocities and deformation, and (3) to test the influence of the width of plates and the initial separation between them on the evolution of the system.

2. Model Setup

2.1. Assumptions

In this work we have adopted an experimental setup widely used in analog modeling of subduction processes (e.g., Becker et al., 1999; Bellahsen et al., 2005; Faccenna et al., 1996; Funiciello et al., 2003; Griffiths et al., 1995; Guillou-Frottier et al., 1995). Thereby, the analog models presented in this study are based on the following assumptions:

The slab is modeled as a viscous body. We further simplify the slab and mantle rheologies using a Newtonian fluid although experimental data suggest that in the natural prototype the upper mantle materials can also follow a nonlinear rheology in regions of large stress (Brace & Kohlstedt, 1980).

The system is isothermal. This is equivalent to considering that the slabs are in a quasi-adiabatic condition, which is a good approximation as long as the subduction velocities are greater than 1 cm/year (Bunge et al., 1997; Wortel, 1982).

Slab pull is the only driving force acting on the experimental system. No external boundary conditions acting on the trenches are applied. The velocity of plates is forced to be zero at their trailing edges such that the retreating rate equals the amount of subduction ($v_s = v_t$, Figure 2) if internal deformation is negligible. This condition maximizes the effects associated with toroidal flow and is therefore an upper bound in quantifying its effects.

Despite the overriding plate is of large influence on subduction evolution (Yamato et al., 2009), we do not include it into the setup in order to run simplified models with clear cause-effect relationships. Hence, we use the same low viscosity as the mantle for all the plate boundaries. This assumption implies that the overriding plates move passively with the retreating trenches.

The experimental setup uses a Plexiglas bottom to simulate the 660-km discontinuity. This implies that the upper-lower mantle boundary is considered as impermeable. This choice is justified by the fact that the lower mantle viscosity is at least one order of magnitude higher than the upper mantle, and the timescale of the process is of the order of a few tens of millions of years (e.g., Christensen, 1996; Davies, 1995; Funiciello et al., 2003; Guillou-Frottier et al., 1995).

There is no imposed mantle flow in the experimental setting as we are interested to isolate the mantle advection produced by the slabs. Hence, the only momentum within the mantle is that caused by the plate/slab system.

The reference frame of these models is the box boundary, which can be considered as the experimental analog of the mantle reference frame.

2.2. Materials and Scaling Parameters

The double subduction system is approximated by two linear viscous layers representing the oceanic plates and the upper mantle. The oceanic plates are made by silicone putty (pure silicone with ~42 wt% Fe fillings to obtain the required density), which is a viscoelastic material that at experimental strain rates acts as a Newtonian high-viscosity fluid (Ten Grotenhuis et al., 2002; Weijermars, 1986). The upper mantle is approximated by a syrup that behaves as a Newtonian low-viscosity and high-density fluid (Schellart & Moresi, 2013).

Our models have been scaled respecting the standard scaling procedure used in stress scaled down for length, density, and viscosity in a natural gravity field ($\vec{g}_{\text{model}} = \vec{g}_{\text{nature}}$; e.g., Weijermars & Schmeling, 1986). A summary of the parameters used in the models and their corresponding values in nature is shown in Table 1. The scale factor for length is 1.6×10^{-7} (1 cm in the experiment corresponds to 60 km in nature). The scale density contrast between the oceanic plate and the upper mantle is $\rho_l \rho_m \approx 60$ kg/m^3, whereas the average viscosity ratio is $\eta_l/\eta_m = 215$. These values are close to those estimated in nature which range from 40 to 80 kg/m^3 for the density contrast and from 10^2 to 10^3 for the viscosity ratio (e.g., Funiciello et al., 2008; Schellart, 2008; Stegman et al., 2010). With these scale ratios, we calculated that 1 min in the evolution of the model corresponds to 1 Myr in nature.

Kinematic parameters are normalized to obtain dimensionless quantities to simplify the comparison of results from different models. Trench velocities are normalized by the Stokes velocity v_s, which is specific for each experiment:

$$v_{norm} = \frac{v}{v_S} = \frac{v}{(\rho_l - \rho_m)\cdot g \cdot H \cdot h/\eta_m}$$

where v is the measured velocity, g is the gravity acceleration, ρ_l is the plate (silicone) density, ρ_m is the mantle (syrup) density, h is the oceanic lithosphere thickness, H is the mantle thickness, and η_m is its viscosity. As pointed out by Capitanio et al. (2007), the normalized velocity is also a measure of the slab geometry such

Table 1
Scaling of Parameters in Laboratory and in Nature for the Presented Experiments

Parameter	Symbol	Units	Laboratory	Nature
Gravitational acceleration	g	m/s^2	9.81	9.81
Upper mantle thickness	H	m	0.11	660,000
Oceanic lithosphere thickness	h	m	0.0135–0.0145	81,000–87,000
Lateral distance between plates	d	m	0.005–0.1	30,000–600,000
Density contrast	$\Delta\rho = \rho_l - \rho_m$	kg/m^3	60	~75
Viscosity ratio	η_l/η_m	–	188–256	10^2–10^3

that for our case, in which subduction occurs purely due to trench retreat, v_{norm} = 1/tan (α) being α the dip angle of the slab. Therefore, higher v_{norm} results in smaller slab dip.

Time is normalized relative to the time taken by the slab to arrive at the lower mantle (t') according to a single plate reference model,

$$t_{norm} = \frac{t}{t'}$$

In our case, t' = 20 min.

2.3. Experimental Procedure and Measurements

Experiments were designed to analyze the behavior of a double subduction system with opposite retreating directions in adjacent plate segments. We perform the experiments in a 150 × 150 × 50 cm^3 Plexiglas tank filled with high-density and low-viscosity syrup, simulating the mantle as a Newtonian fluid (Figure 3). An impermeable layer is placed at 11-cm depth as analog of the upper-lower mantle boundary. Plates are fixed at their trailing edge, and subduction is started by deflecting simultaneously the leading edge of both plates inside the syrup up to a depth of 3 cm (~200 km in nature). We run 12 analog experiments with two slabs varying the width of the plates and the distance between them. Additionally, we run six single-plate subduction models as reference examples, two of them including a stationary side plate to investigate the role of the

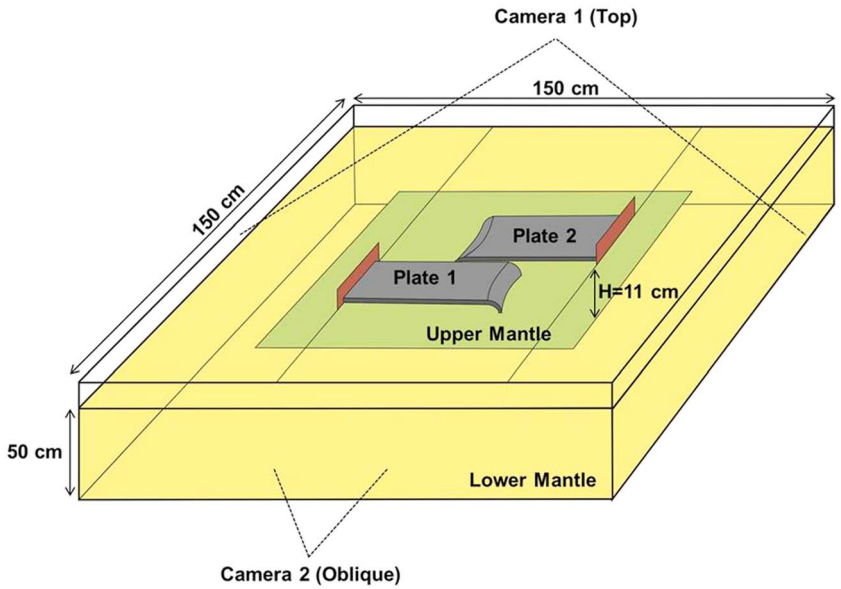

Figure 3. Scheme of the experimental setup. The tank is full of viscous syrup (in yellow) representing the mantle. The oceanic plates are made by silicone putty and subduct in opposite directions. Both plates are fixed at their trailing edge to enforce slab rollback. A fixed base (in green) is placed at 11-cm depth to simulate the upper-lower mantle transition. Two cameras are placed above the experiment (camera 1) and in an oblique position (camera 2) to observe the evolution of the system.

Table 2
Geometric Characteristics and Physical Parameters of the Laboratory Experiments

Double subduction models											
		Plate 1		Plate 2							
Experiment	d_0(cm)	w (cm)	h (cm)	w (cm)	h (cm)	ρ_l (kg/m^3)	ρ_m (kg/m^3)	η_l (Pa s)	η_m (Pa s)	η_l/η_m	V_{Stokes} (mm/min)
E1	2	10	1.30	10	1.30	1499	1445	40470	216	188	211
E2	1	10	1.40	10	1.40	1499	1445	40049	213	188	230
E3	0.5	10	1.30	10	1.30	1499	1445	40530	211	192	215
E4 – Model 4	0.5	10	1.35	10	1.35	1499	1445	40470	213	190	219
E5	0.5	20	1.35	20	1.35	1499	1445	40771	202	202	234
E6 – Model 3	0.5	20	1.40	20	1.40	1511	1445	38728	151	256	396
E7 – Model 2	0.5	30	1.40	30	1.40	1499	1445	39929	195	205	251
E8	10	10	1.33	10	1.33	1511	1445	39509	176	224	322
E9	10	20	1.40	20	1.40	1511	1445	39809	174	229	344
E10 – Model 1	10	30	1.45	30	1.45	1511	1445	39929	179	223	347
E11 – Model 5	0.5	30	1.40	10	1.35	1511	1445	38968	172	227	341
E12	10	30	1.40	10	1.40	1511	1445	39689	167	237	358
Single subduction with lateral fixed plate											
E13 – P2 fixed	0.5	20	1.40	20	1.35	1511	1445	39268	167	235	350
E14 – P2 fixed	0.5	20	1.40	20	1.40	1511	1445	38908	163	239	368
Single Subduction (Reference models)											
Experiment		w (cm)		h (cm)		ρ_l (kg/m^3)	ρ_m (kg/m^3)	η_l (Pa s)	η_m (Pa s)	η_l/η_m	V_{Stokes} (mm/min)
E15		10		1.35		1,499	1,445	40,530	209	194	226
E16		20		1.35		1,499	1,445	40,170	204	197	231
E17		20		1.35		1,511	1,445	38,968	167	233	345
E18		30		1.35		1,511	1,445	40,290	206	195	280

adjacent passive lithosphere. Table 2 summarizes the model experiments indicating the geometric characteristics and the relevant physical parameters.

The width of the plates varies from 10 to 30 cm (600 to 1,800 km in nature) and the initial distance between them varies from 0.5 to 10 cm (30 to 600 km in nature). A grid of 1×1 cm^2 is drawn on the upper surface of each plate to quantify the deformation during the evolution of the model.

Models are monitored with two cameras taking photographs every 30 s from the top and an oblique position with respect to the model. We use postprocessing tools on the photos to analyze the trench retreat velocities, the trench curvatures, and the lateral distance between plates during the experiment. Moreover, the toroidal mantle flow is observed on the top-view photos through the microbubbles created in the syrup to track the fluid movement and quantified using the Particle Image Velocimetry technique (i.e., PIVlab software; Thielicke & Stamhuis, 2014).

We calculate the trench retreat velocities of each plate by tracking the location of the two edges and the center of the trench. The retreating rate is calculated as a weighted average of these points to reduce the effect that the increase in trench curvature can cause on the apparent trench retreating rate. In order to quantify the trench curvature we represent the trench geometry as a circular segment. The curvature c is then defined as

$$c = \frac{r_2}{r_1}$$

where r_1 is the chord and r_2 is the sagitta of the section (Figure 4). The curvature is therefore zero for a straight trench, and it increases for curved trenches.

The lateral displacement of the plates is measured by quantifying the variations of the distance l between the centers of the trenches (Figure 4).

It is worth noting that as in any experimental approach, internal inhomogeneities of the materials and laboratory procedures could introduce spurious uncertainties in the results. The noise observed in the data is mainly a consequence of the inevitable unevenness and nonuniformity in making up the

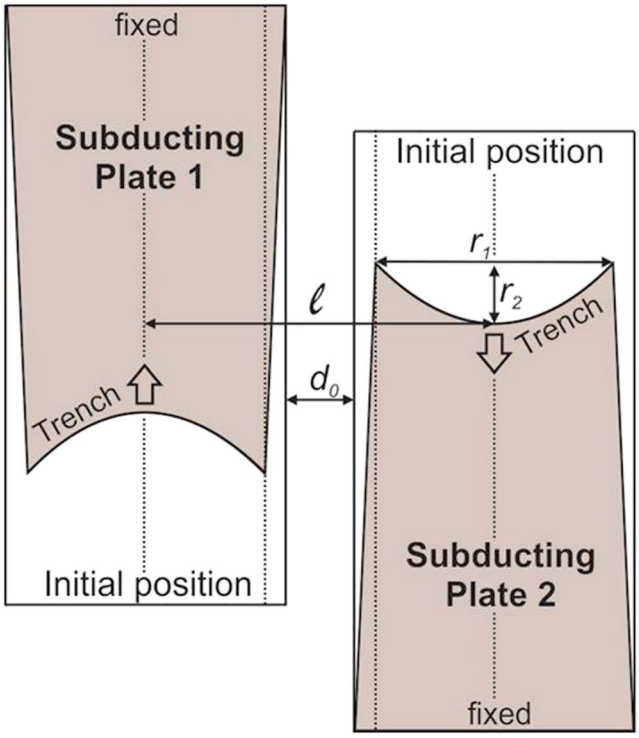

Figure 4. Simplified sketch of the model setup (top view). Plates are fixed at their trailing edge. The initial separation between plates (d_0) is the distance between the lateral edges before subduction starts. The lateral distance between plates (l) is defined as the perpendicular distance between the centers of the trenches. The trench curvature (c) is defined as r_2/r_1.

experimental setup. Despite these limitations, the experimental results presented in the following section are robust enough to shed light on the dominant processes involved in the models.

3. Results

To understand the results of our experiments, we must recall that the basic kinematics of single-plate subduction processes results from the balance of the acting forces that in the absence of the upper plate includes gravitational slab pull, viscous shear with the ambient mantle, and viscous resistance energy term to downward plate bending (Figure 2). Alike numerous analog and numerical experiments with fixed trailing edge ($v_s = v_t$; e.g., Funiciello et al., 2003; Schellart, 2004), our single-plate models (E15 to E18; Table 2) show a characteristic evolution of the subducting lithosphere during its descent into the upper mantle and its interaction with the 660-km discontinuity. This evolution can be divided in three phases characterized by different trench kinematics. During the first phase of the experiment, before the slab reaches the bottom of the upper mantle, the trench retreats with a fast rate that increases progressively in time with the amount of subducted material. Then there is a short period of low trench retreat velocity during which the leading edge of the slab bends and accommodates on the upper/lower mantle discontinuity. Finally, the trench/slab retreat follows a steady state velocity regime until subduction is completed. Trench/slab retreat generates a symmetric pattern of mantle flow with active poloidal and toroidal components (e.g., Funiciello et al., 2003, 2006; Schellart, 2004; Strak & Schellart, 2014). The toroidal component is due to the pressure difference between the mantle at the topside and the bottomside of the slab leading to mantle flow around the slab edges toward the topside. This results in a concave curvature of the trench toward the mantle wedge, which increases with the trench retreat and decreases with increasing the viscosity ratio between the slab and the upper mantle (e.g., Morra et al., 2006, 2009; Schellart, 2010). We focus our study on phases 2 and 3 of double subduction systems as defined in Király et al. (2016), in which steady state subduction has been reached (see section 1), and we analyze the variations of the trench retreat velocities and the trench curvature as a function of time.

In order to illustrate the most outstanding results we have selected five models (Table 2) showing the role of the initial separation between plates, how the mantle flow is modified in such double subduction system, and the effects of the plate width.

3.1. Model 1: Wide and Distant Plates

Model 1, composed of two plates of 30-cm width and spaced 10 cm, is designed to study the behavior of the system when the interaction between plates is very weak. In this model plates are slightly thicker (1.45 cm; Table 2) than in the rest of the models and the viscosity contrast between the plates and the mantle is $\eta_l/\eta_m = 223$ (Table 2). Figure 5 shows the normalized trench retreat velocity v_{norm} and the trench curvature c of both plates as a function of the normalized time t_{norm}. Velocities keep almost constant during phases 2 and 3 showing similar values for both plates ($0.47 \pm 0.04 \cdot 10^{-2}$). The trench curvatures of both plates increase linearly with time showing nearly symmetric shapes and values. Comparing this model with its corresponding reference model (single subduction system of a 30-cm width plate, model E18 in Table 1), we obtain a very similar behavior in terms of retreating velocity and the trench symmetry. Finally, the distance l (see on Figure 4) between the trenches' centers remains roughly constant during the whole experiment indicating that there is no net separation between plates.

3.2. Model 2: Wide and Near Plates

Model 2 is composed of two 30-cm-wide plates with an initial separation of $d_0 = 0.5$ cm. We use this model, alongside with Model 1, to study the influence of the initial separation between plates on the dynamics of the

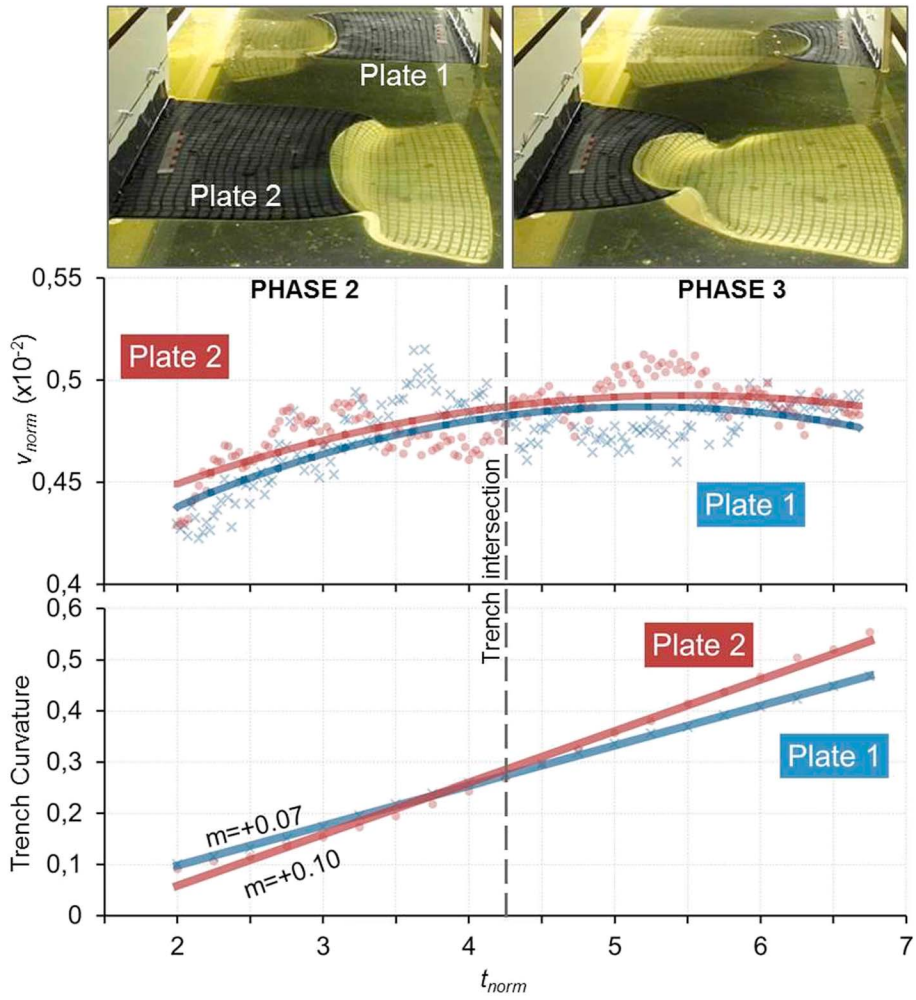

Figure 5. Evolution of double polarity subduction Model 1 during phase 2 (approaching trenches) and phase 3 (diverging trenches). Both plates are 30 cm wide with an initial separation between them of d_0 = 10 cm. Upper and lower graphics show the normalized retreating velocity and curvature of the trenches vs normalized time (see text). The crosses and dots indicate measurements, and the thick lines correspond to a second-order polynomial regression (upper graphic) and linear regression (lower graphic).

mantle flow and plates interaction. Figure 6 shows the normalized trench retreat velocity and trench curvature of both plates as a function of the normalized time.

The most outstanding effect of reducing the initial separation between plates is the acceleration/deceleration of the retreat velocities and the variation with time of the distance between plates. Velocities tend to increase during the trench-approaching phase 2 varying from around $0.42 \cdot 10^{-2}$ to $0.62 \cdot 10^{-2}$ and decrease to $0.52 \cdot 10^{-2}$ during phase 3 while trenches diverge. Since $v_{\text{norm}} = 1/\tan(\alpha)$ we should expect that during phase 2 the dip angle decreases as the normalized trench velocity increases, whereas in phase 3 the dip angle increases as trench velocity decreases. Unfortunately, the experiments do not allow measuring the evolution of the dip angle with enough accuracy and we cannot confirm this aspect. Alike Model 1, the curvature of the trenches increases linearly with time. Both, normalized trench velocities and curvatures reach slightly higher values than in Model 1.

The lateral distance between plates l increases during phase 2 resulting in a maximum increment of Δl = 0.4 cm or 1.3% relative to the initial position. During phase 3, l decreases progressively as the trenches approach the trailing edge of the respective plates, which are subjected to fixed boundary conditions.

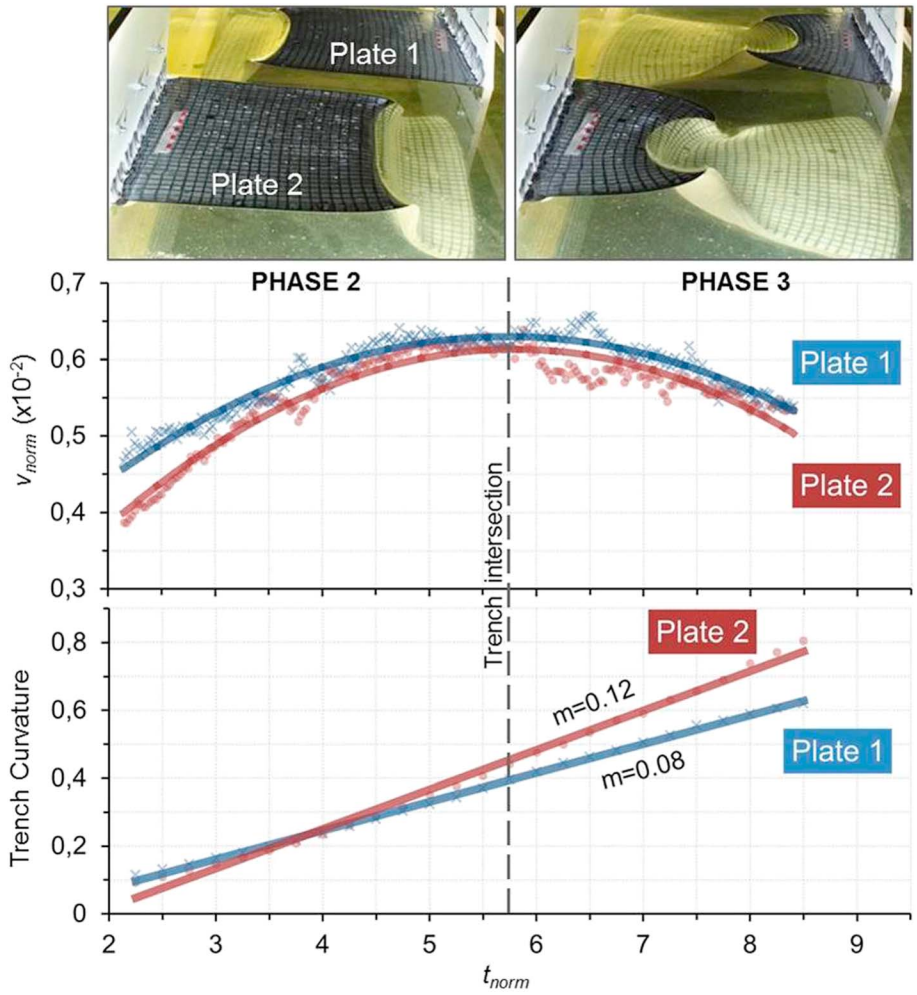

Figure 6. Evolution of double polarity subduction Model 2 during phase 2 (approaching trenches) and phase 3 (diverging trenches). Both plates are 30 cm wide with an initial separation between them of $d_0 = 0.5$ cm. The upper and lower graphics show the normalized retreating velocity and curvature of the trenches vs normalized time (see text). The crosses and dots indicate measurements, and the thick lines correspond to a second-order polynomial regression (upper graphic) and linear regression (lower graphic).

3.3. Model 3: Induced Toroidal Mantle Circulation

Model 3 is chosen to show how the toroidal component of the mantle flow and the plate deformation patterns are modified in a double subduction system. The model consists of two 20-cm-wide plates with an initial separation of 0.5 cm. The top camera allows tracking the syrup flow through the movement of exposed microbubbles in a horizontal section at ~1-cm depth as well as the deformation of the subducting plates observing the distortion of the grid drawn on their surfaces. The patterns obtained in this model can be extrapolated to the rest of the tested configurations. Figure 7 shows the inferred horizontal displacements occurring in the syrup (red arrows) and the plates (white arrows) before, during, and after trenches pass each other.

During phase 2 (Figure 7a), the mantle flow delineates toroidal convective cells around the outer edges of the trenches of both plates whereas in the inner edges, the convective cells are less vigorous. Linked to these toroidal cells, there is an outward flow perpendicular to the outer sides of the plates, which tends to vanish in the region between both plates because the cells have opposite polarity, particularly when the trenches align with each other. The divergent displacement of both plates, indicated by the white arrows, is the combination of the stress perpendicular to the trench generated by the slab pull, and the drag produced by the outward flow of the syrup.

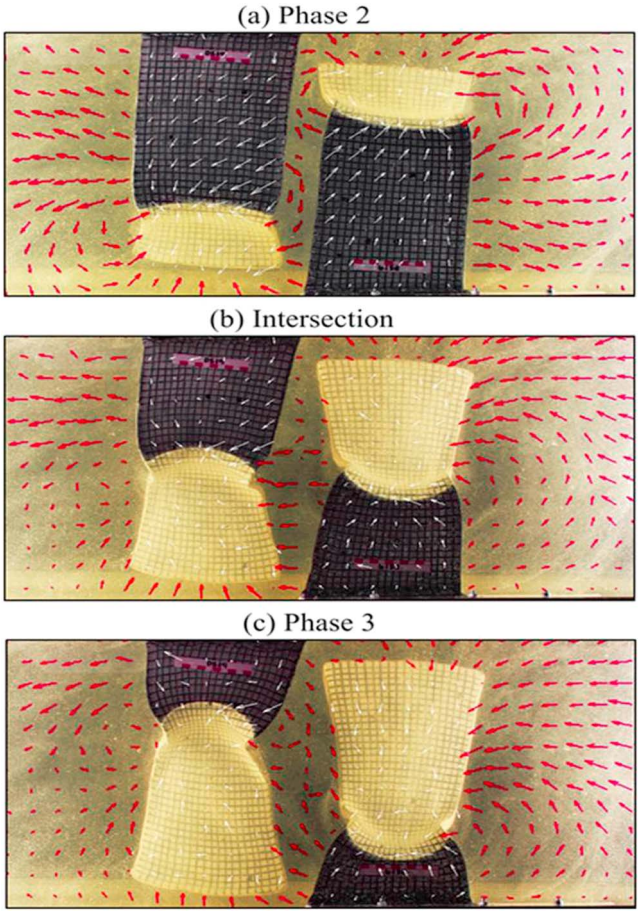

Figure 7. Syrup (mantle) flow (red arrows) and plate deformation (white arrows) corresponding to Model 3 (Table 2) during approaching (a) trench phase 2, (b) trench intersection, and (c) diverging trench phase 3.

In the transition from phases 2 to 3 (Figure 7b), the toroidal flow around the outer edges of the trenches persists. The perpendicular distance *l* between the centers of the trenches (see Figure 4) becomes higher, and the region between the plates is occupied by a single convective cell in which the outward flow of the syrup from the central parts of one plate is directed to the trench of the opposite plate and vice versa. The displacement of the plates depicted by the white arrows is quite random being well defined only near the trenches.

During phase 3 (Figure 7c), the toroidal flow around the outer edges of the trenches appears well defined, and as most of the plate is already subducted and the trench approaches the fixed trailing edge, the lateral outward drag is less vigorous. The flow in the interplate region is weakened and actually vanished in its center because of the opposite directions of the generated toroidal cells around the inner edges of the trenches.

3.4. Model 4: Narrow and Near Plates

Model 4 is composed of two 10-cm-wide plates with an initial separation distance of $d_0 = 0.5$ cm and is designed to analyze the effects of the plate width on the dynamics of the system. The behavior of the system (Figure 8) is very similar to that for wide and near plates (Model 2) with similar normalized velocities and slightly lower acceleration/deceleration, indicating that the retreating velocity is not very sensitive to the width of plates. In contrast, the curvature of the trenches is almost three times lower for the narrow plates.

The normalized retreating velocity during phase 2 increases from around $0.50 \cdot 10^{-2}$ to $0.67 \cdot 10^{-2}$ for plate 1 and from around $0.43 \cdot 10^{-2}$ to $0.55 \cdot 10^{-2}$ for plate 2. During phase 3 the normalized retreating velocity of plate 1 decreases to $0.55 \cdot 10^{-2}$, whereas for plate 2 the retreating velocity decreases to $0.45 \cdot 10^{-2}$. Trench curvature of both plates increases linearly during all the retreating process disregarding the relative position of the trenches. However, results show a larger curvature for plate 2. The correlation between trench retreating velocities and trench curvature of both plates suggests that the higher the velocity is, the smaller the curvature is (Figure 8). The noticeable distinct behavior between the two plates may be due to small differences in plate thickness (±0.5 mm), since these are within the possible variability of the experimental setup and suffice to produce the observed velocity variations.

The lateral distance between plates increases during phase 2 ($\Delta l = 0.5$ cm), resulting in a maximum increment of ~5% from its initial value. During phase 3, *l* decreases, what is forced by the fixed position of the back edge of plates.

3.5. Model 5: Wide/Narrow Near Plates

Model 5 is designed to study the interaction of two near subducting plates ($d_0 = 0.5$ cm) with different widths. In this case we have considered 30 and 10 cm for plates 1 and 2, respectively. Figure 9 shows that the normalized trench retreating velocity for the wider plate 1 increases during phase 2 from $0.46 \cdot 10^{-2}$ to $0.55 \cdot 10^{-2}$ keeping this value almost constant during phase 3. In contrast, the narrower plate 2 shows a smooth variation of the normalized velocity around an average value of $0.43 \cdot 10^{-2}$ during both phases. A weak relative maxima velocity of $0.46 \cdot 10^{-2}$ during phase 3 at $t_{norm} = 4.5$ can be identified in Figure 9.

The trench curvature of both plates increases linearly with time, showing maximum curvatures of 0.56 for plates 1 and 0.28 for plate 2. While plate 1 shows a nearly symmetric shape, the narrower plate 2 is affected by the near plate 1 slab, and undergoes an asymmetric deformation. The distance between plates *l* increases (Δl = 0.8 cm, i.e., 3.9% from the initial position) during phase 2 and decreases during phase 3

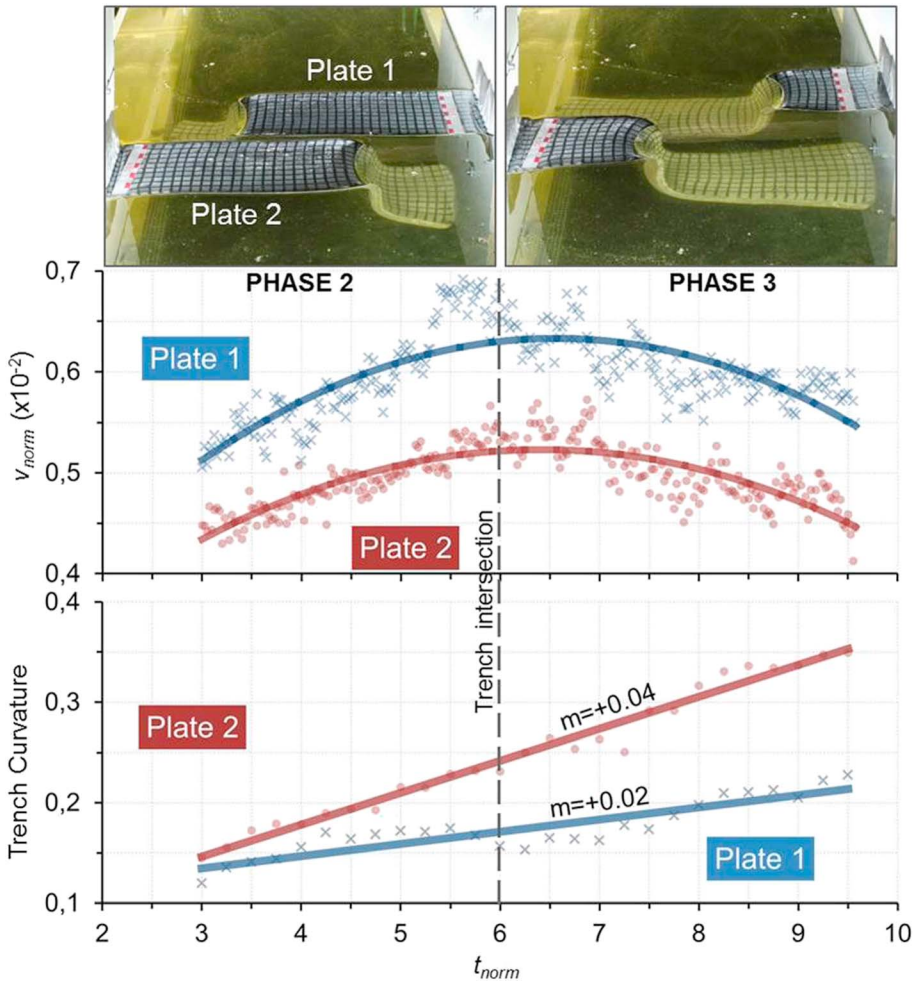

Figure 8. Evolution of double polarity subduction Model 4 during phase 2 (approaching trenches) and phase 3 (diverging trenches). Both plates are 10 cm wide with an initial separation between them of $d_0 = 0.5$ cm. The upper and lower graphics show the normalized retreating velocity and curvature of the trenches vs normalized time (see text). The crosses and dots indicate measurements, and the thick lines correspond to a second order polynomial regression (upper graphic) and linear regression (lower graphic).

forced by the fixed position at their trailing edges. This lateral displacement is essentially undergone by the narrower plate 2.

4. Discussion

We have grouped the main distinct features characterizing the double plate subduction system in three main topics.

4.1. Induced Mantle Flow

The main difference between the double-plate subduction system presented here and most of the earlier mentioned double-subduction studies is that in our models the plates are located side by side and retreating in opposite directions. As a result, the interaction between the individual flow cells associated with each plate produces two effects on the combined mantle flow: (i) the flow is not symmetrical with respect to the longitudinal axis of each plate and (ii) the opposed retreating directions preclude a steady state phase of the subduction process.

Figure 10 is an idealized cartoon, based on the syrup particle tracks recorded in the different experiments (e.g., Figure 7), illustrating the evolution of the mantle flow generated by the double-plate system. Once

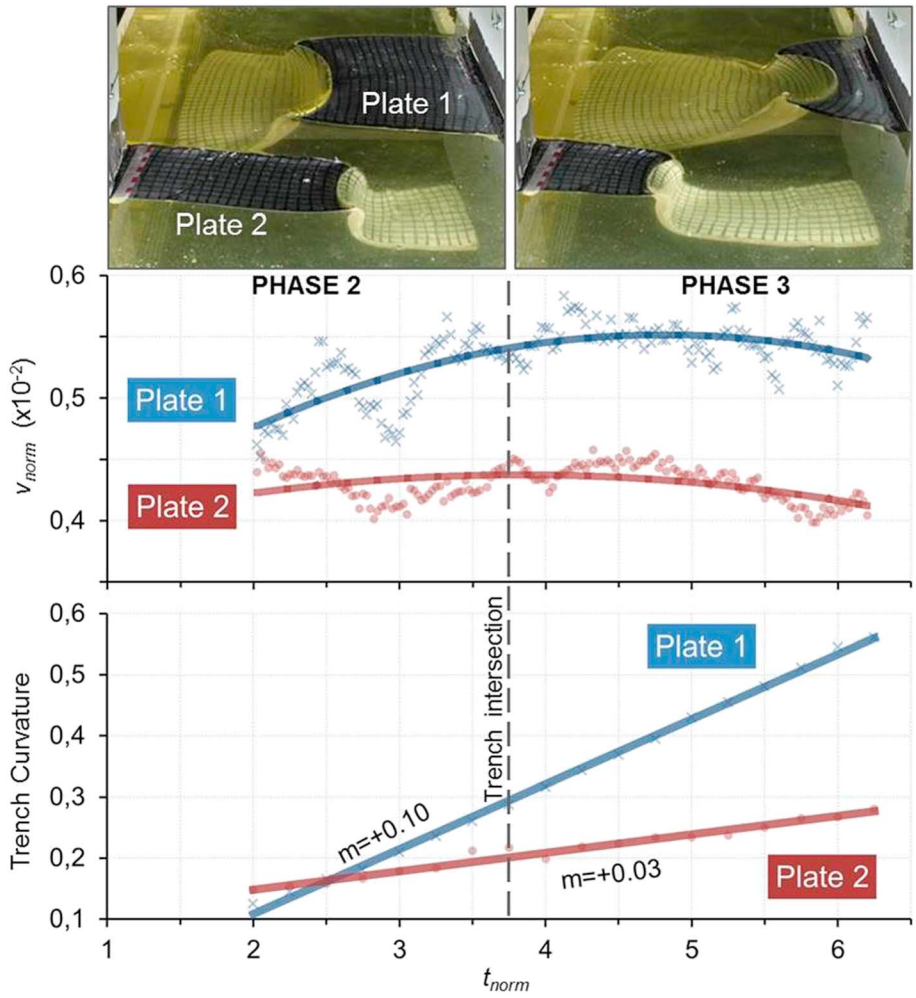

Figure 9. Evolution of double polarity subduction Model 5 during phase 2 (approaching trenches) and phase 3 (diverging trenches). Plates 1 and 2 are 30 and 10 cm wide, respectively, with an initial separation between them of $d_0 = 0.5$ cm. Upper and lower graphics show the normalized retreating velocity and curvature of the trenches vs normalized time (see text). The crosses and dots indicate measurements, and the thick lines correspond to a second-order polynomial regression (upper graphic) and linear regression (lower graphic).

the plates have reached the impermeable layer at 11-cm depth simulating the upper-lower mantle boundary, the toroidal flow becomes the dominant mantle circulation component especially under fixed trailing edge conditions (e.g., Stegman et al., 2006). These conditions define an end-member subduction setting where toroidal flow is maximal. The toroidal cells generated by the retreating slabs have opposite directions, and their encounter induces a shear zone along the region between the two plates. The resulting asymmetric flow beneath each plate causes a net lateral mantle drag that tends to separate the plates (Figure 10a). As the two trenches retreat, the more external streamlines merge into a coherent toroidal convective cell connecting both trenches in a progressive feedback process that accelerates the trench retreat (Figure 10b). When the trenches become aligned, the toroidal cells merge into one cell and all the streamlines in the interplate region follow the same direction producing the maximum trench retreat velocities (Figure 10c). As the trenches move away from each other, the toroidal cells related to each slab in the inter-plate region tend to become independent reactivating the shear zone and slowing the trench retreat (Figures 10d and 10e). The mantle flow interaction in the interplate region becomes less and less active until subduction is completed.

This general behavior of the mantle has been described in Király et al. (2016), but unlike the analog models presented here, their numerical study does not show the progressive separation between the plates' centers.

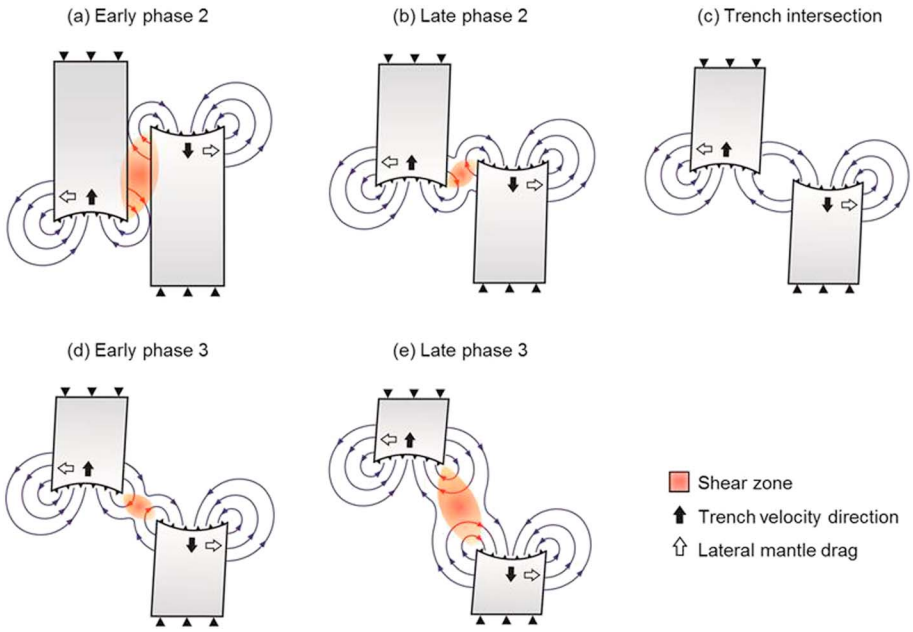

Figure 10. Idealized cartoon illustrating the evolution of the mantle flow generated by a double-plate system with opposite subduction polarity in adjacent segments. The opposite directions of the return flow in the interplate region generate a shear zone that tends (a–c) to vanish as the trench approach and (d and e) to increase again as the trenches diverge until subduction completes.

This is because only the half of the plates is modeled with their symmetry axis coinciding with the sidewalls of the model, which are subjected to free-slip boundary thus suppressing trench parallel motion. It must be noted, however, that the separation of plates is favored by the absence of lithosphere at both sides of the double plate system. Despite this is an unrealistic condition in nature, the extensional stresses generated by the asymmetric mantle flow will persist, whereas the possible shallow effects of the extension perpendicular to the plates are more debatable.

4.2. Plate Interactions

The possible interactions between plates are associated with the stress propagation through the induced mantle flow, and therefore, the initial separation between plates must play a relevant role in the evolution of this double plate system. Comparing the normalized trench retreating velocities obtained for configurations with distant plates (Model 1; Figure 5) and near plates (Models 2 and 4; Figures 6 and 8), we observe that the velocity variations are related to the initial plate separation d_0 such that the nearer the plates are the higher the variation is. Actually, experiments with near plate configurations show an acceleration and deceleration in the trench retreat during phases 2 and 3, respectively. Maximum velocities are attained close to the moment when the trenches align with each other. In contrast, distant plate configurations show roughly steady state trench retreat velocities. This is in agreement with the results obtained by Király et al. (2016) showing that when plates are separated by distances larger than 600 km (10 cm in our experiments) the interaction between plates is negligible. Interestingly, Model 5, encompassing near wide (30 cm) and narrow (10 cm) plates, shows also roughly steady state retreating velocities (Figure 9). The possible reason lies in the negligible effect that the narrow plate 2 produces on the wider plate 1. Consequently, plate 1 behaves as an independent single plate pushing outward plate 2 and causing small variations in its retreating velocities due to the large separation created between both plates. On the other hand, the strong toroidal flow related to plate 1 largely deforms the other, narrow plate.

The interaction between near plates generates a progressive lateral separation between the trench centers, which is more noticeable for narrow plates as evidenced by comparing Models 2 and 4. Plate separation is a measure of the lateral deformation of plates, which depends on the drag exerted by the mantle flow and the

bending resistance related to plate viscosity such that the narrower the plates are, the larger the lateral separation between them is.

The trench curvature appears to be independent on the initial separation of plates and therefore on the plate interaction related to the opposite subduction polarity process, as evidenced by comparing Models 1 and 2 (Figures 5 and 6). A consequence of this is that trench curvature increases steadily throughout phases 2 and 3 as observed in all models. Note that the variations in the normalized trench retreating velocities are very low producing an unnoticeable change in the curvature trend line. Near-plate configurations seem to produce asymmetric trench curvatures though we cannot ascertain whether they are a consequence of the asymmetry in the generated mantle flow or to spurious errors in the experiment setup. By comparing Models 2 and 4 (Figures 6 and 8) and Models 1 and 5 (Figures 5 and 9), we observe that the trench curvature mainly depends on the plate width such that wider plates show larger curvatures in agreement with previous works (e.g., Funiciello et al., 2003; Schellart, 2010). Trench curvature also depends strongly on the viscosity ratio between plates and underlying syrup, and although our study is not designed to systematically analyze this dependence, we observe that trench curvature in experiment E5 (Table 1; $\eta_l/\eta_m = 202$) is significantly greater than in experiment E6 (Table 1; $\eta_l/\eta_m = 256$), with similar values for all the other parameters. Therefore, differences in curvature between Models 1 and 2 can be due to small variations in the viscosity ratio η_l/η_m (Table 2). The curvature values calculated for the latest stages of Model 2, with plates 30 cm wide, are close to $c = 0.8$ meaning that the arc delineated by the trenches corresponds to three fourths of the circumference. Such closed arc-trenches are not easily observed in nature, where tightest arcs (e.g., Gibraltar Arc, Calabrian Arc, Scotia Arc, Caribbean Arc, Banda Arc, and Carpathians Arc) show maximum values of $c = 0.4$–0.5. This discrepancy between analog models and nature can be due to the absence of overriding plate in our experiments, which overestimates the curvature of the trench, as proposed by Meyer and Schellart (2013).

4.3. Tectonic Relevance

Though the application of the obtained results to natural cases is not straightforward due to the necessary simplifications of the tested analog models, we can analyze some of their consequences in terms of distribution of stress, magmatism, and seismic anisotropy. A suitable region to test the effects of opposite subduction polarity in adjacent plate segments is the Central-Western Mediterranean where such process has been described in the Betic-Rif-Tell system (e.g., Casciello et al., 2015; Vergés & Fernàndez, 2012) and in the Alps-Apennines system (e.g., Faccenna et al., 2014; Vignaroli et al., 2008).

The Betic-Rif and the Tell chains and their metamorphic complexes are located at opposed margins in the western Mediterranean, showing opposite tectonic vergences, and separated by the Alboran and the Algerian back arc basins, respectively. According to Vergés and Fernàndez (2012) and Casciello et al. (2015) the slabs retreated in opposite directions and passed each other before reaching the upper-lower mantle boundary. Subduction and related mantle flow produce changes in the rock fabric that results in a complex seismic anisotropy pattern that depends on depth, amount of subduction, slab geometry, trench displacement, and consequent mantle flow (e.g., Di Leo et al., 2014; Faccenda & Capitanio, 2013). SKS-based anisotropy onshore shows a clear alignment of the fast polarization directions (FPD) along strike of most of the Betic-Rif chain (Díaz et al., 2015). Though there are hardly any offshore anisotropy data, a common observation is the pronounced change of FPD from the Alboran to the Algerian basin. Three-dimensional azimuthally anisotropic model of Europe shows FPD orientations changing from WSW-ENE in the Alboran Basin to NW-SE in the Algerian Basin at 70- to 200-km depth (Zhu & Tromp, 2013; see their Figures 1 and S3). In contrast, uppermost mantle anisotropy derived from Pn and Sn tomography shows distinct and almost perpendicular FPD patterns with a prominent NW-SE orientation in the southern margin of the Alboran Basin changing to NE-SW in the Algerian Basin (Díaz et al., 2013; see their Figure 9).

These spatial and vertical anisotropy variations can be explained as the result of the complex interaction between the return flows associated with the opposite retreat of a double subduction system together with the northwest to west tectonic transport of the Betic-Rif units. The volcanic geochemical signature in the western Mediterranean varies from early Oligocene tholeiitic magmatic manifestations of the Malaga dykes to Late Miocene-Quaternary calc-alkaline/HK calc-alkaline and alkaline magmas. This complexity is related to recycling and depletion of rocks due to subduction and rifting events operating in the region, and therefore, the geochemistry of volcanic products does not always correspond to the present-day geodynamic setting in which they are sampled (e.g., Carminati et al., 2012; Lustrino & Wilson, 2007; Lustrino et al., 2011; Melchiorre

et al., 2017). Melchiorre et al. (2017) related the age, location, and type of the widespread volcanism in the western Mediterranean to the different evolutionary stages proposed by Vergés and Fernàndez (2012). It must be said however that the great variety of magmatic compositions and their spatial distribution, as well as the limited availability of offshore anisotropy observations, allow for alternative geodynamic interpretations (e.g., Chertova et al., 2014; Duggen et al., 2005; Faccenna et al., 2004; Spakman & Wortel, 2004; van Hinsbergen et al., 2014).

The Alps-Apennines system has been analyzed by Király et al. (2016) proposing that the stress propagation and mantle flow associated with the interaction between the near retreating Tethyan plate segments likely contributed to the late stages of curvature of the Western Alps and to the slab breakoff. Likewise, the opposite dipping Ryukyu- Manila trenches in the Western Pacific would also be affected by the stress interaction causing the strong curvature of the SW-Ryukyu trench (Király et al., 2016). A complex mantle flow resulting from the interaction of subducting plates with different polarities is derived from numerical modeling (Lin & Kuo, 2016), which is compatible with the tectonic and seismic anisotropy observations in this region. These authors, however, use the present-day geometry of the opposite-verging subduction rather than its time evolution.

Opposite subduction polarities are also present in New Zealand between the Tonga-Kermadec trench dipping to the west beneath the North Island and the Puysegur trench dipping to the east beneath the South Island. The Hikurangi Trough, corresponding to the subduction of the Pacific Plate beneath the North Island, shows a strong curvature and coincides with a fast clockwise rotation of the North Island (Wallace et al., 2004). However, the effect of the interaction between both slabs is more elusive since they are separated at a critical distance of 500–600 km by the right-lateral transpressive Alpine Fault. Furthermore, the subduction in the Northern Island has initiated 25 Ma, whereas in South Island it has started 10–12 Ma (King, 2000). Indeed, Wallace et al. (2009) suggest that the Hikurangi Trough curvature is produced by the collision of the Chatham Rise microplate on the Pacific Plate with the northern South Island.

In summary, the exploratory model experiments stand at relatively large distance from the complex setting and evolution of natural double subduction. Still, the experiments do emphasize that a strong lateral stress coupling can occur between the two oppositely retreating subduction systems. The stress coupling varies in space and time as a function of the relative position between the trenches and may be recorded in mantle anisotropy and, as well, translate into a tectonic response.

5. Concluding Remarks

We have designed a number of laboratory experiments to better understand the dynamics of the plate/mantle interactions in a double subduction system with opposite polarity in adjacent segments. In particular, we have tested the influence of the plate width and the initial separation between plates focusing our analysis on plate deformation described in terms of the evolution of trench retreat velocity and trench curvature, as well as on the variations in the lateral distance between the two plates and the induced mantle flow. From the laboratory experiments presented here we conclude the following:

The mantle flow induced by both plates shows an asymmetrical pattern around both trenches preventing a steady state phase of the subduction process to occur. Variations of observed rollback velocities and plate separation strongly correlate with the evolution of the toroidal cells around the inner edges of the trenches.

The critical initial plate separation beyond which the interaction between the two slabs vanishes is about 10 cm in the experiments, or ~600 km in nature, thus confirming previous numerical results.

For initial plate separations smaller than the critical distance, trench retreat velocities increase while trenches approach (phase 2) and decrease while trenches diverge (phase 3), reaching a maximum velocity close to the trench alignment. The velocity variation is proportional to the width of the plates.

The trench curvature increases linearly with time in all models. This trend line, which depends on the viscosity ratio and the return mantle flow balance, is independent of the width of the plates and of the initial plate separation.

The basics of the interaction between opposite subducting adjacent plates can provide relevant clues to better understand the tectonic evolution of natural scenarios despite the oversimplification of the presented models.

Acknowledgments
We are indebted to W. Spakman and an anonymous reviewer and the Associated Editor for their thorough review and the comments and suggestions made, which have largely improved the manuscript. The work of M. P., M. F., and J. V. is part of the projects ALPIMED (PIE-CSIC-201530E082) and MITE (CGL2014-59516-P) and partly financed by the Generalitat de Catalunya (2014-SGR-1471 and 2017-SGR-847). The work of S. Z. is funded by the Spanish Ministry of Economy and Competitiveness through grant CICYT DPI2017-85139-C2-2-R and Generalitat de Catalunya (2017-SGR-1278). All the data used are archived in GFZ Data Services. http://doi.org/10.5880/fidgeo.2018.015.

References

Baumann, C., Gerya, T. V., & Connolly, J. A. D. (2010). Numerical modelling of spontaneous slab breakoff dynamics during continental collision. *Geological Society Special Publication*, *332*, 99–114.

Becker, T. W., Faccenna, C., O'Connell, R. J., & Giardini, D. (1999). The development of slabs in the upper mantle: Insights from numerical and laboratory experiments. *Journal of Geophysical Research*, *104*, 15,207–15,226. https://doi.org/10.1029/1999JB900140

Bellahsen, N., Faccenna, C., & Funiciello, F. (2005). Dynamics of subduction and plate motion in laboratory experiments: Insights into the "plate tectonics" behavior of the Earth. *Journal of Geophysical Research*, *110*, B01401. https://doi.org/10.1029/2004JB002999

Brace, F. W., & Kohlstedt, D. L. (1980). Limits on lithospheric stress imposed by laboratory experiments. *Journal of Geophysical Research*, *50*, 6248–6252. https://doi.org/10.1029/JB085iB11p06248

Bunge, H. P., Richards, M. A., & Baumgardner, J. R. (1997). A sensitivity study of three-dimensional spherical mantle convection at 108 Rayleigh number: Effects of depth-dependent viscosity, heating mode, and an endothermic phase change. *Journal of Geophysical Research*, *102*, 11,991–12,007. https://doi.org/10.1029/96JB03806

Capitanio, F. A., Faccenna, C., Zlotnik, S., & Stegman, D. R. (2011). Subduction dynamics and the origin of Andean orogeny and the Bolivian orocline. *Nature*, *480*(7375), 83–86. https://doi.org/10.1038/nature10596

Capitanio, F. A., & Morra, G. (2012). The bending mechanics in a dynamic subduction system: Constraints from numerical modelling and global compilation analysis. *Tectonophysics*, *522-523*, 224–234. https://doi.org/10.1016/j.tecto.2011.12.003

Capitanio, F. A., Morra, G., & Goes, S. (2007). Dynamic models of downgoing plate-buoyancy driven subduction: Subduction motions and energy dissipation. *Earth and Planetary Science Letters*, *262*(1–2), 284–297. https://doi.org/10.1016/j.epsl.2007.07.039

Capitanio, F. A., Morra, G., & Goes, S. (2009). Dynamics of plate bending at the trench and slab-plate coupling. *Geochemistry, Geophysics, Geosystems*, *10*, Q04002. https://doi.org/10.1029/2008GC002348

Carminati, E., Lustrino, M., & Doglioni, C. (2012). Geodynamic evolution of the central and western Mediterranean: Tectonics vs. igneous petrology constraints. *Tectonophysics*, *579*, 173–192. https://doi.org/10.1016/j.tecto.2012.01.026

Casciello, E., Fernandez, M., Vergés, J., Cesarano, M., & Torne, M. (2015). The Alboran Domain in the Western Mediterranean evolution: The birth of a concept. *Bulletin de la Société Géologique de France*, *186*(4-5), 371–384. https://doi.org/10.2113/gssgfbull.186.4-5.371

Chertova, M. V., Spakman, W., Geenen, T., van den Berg, A. P., & van Hinsbergen, D. J. J. (2014). Underpinning tectonic reconstructions of the western Mediterranean region with dynamic slab evolution from 3-D numerical modeling. *Journal of Geophysical Research: Solid Earth*, *119*, 5876–5902. https://doi.org/10.1002/2014JB011150

Christensen, U. R. (1996). The influence of trench migration on slab penetration into the lower mantle. *Earth and Planetary Science Letters*, *140*(1–4), 27–39. https://doi.org/10.1016/0012-821X(96)00023-4

Čížková, H., & Bina, C. R. (2015). Geodynamics of trench advance: Insights from a Philippine-Sea-style geometry. *Earth and Planetary Science Letters*, *430*, 408–415. https://doi.org/10.1016/j.epsl.2015.07.004

Conrad, C. P., & Hager, B. H. (1999). Effects of plate bending and fault strength at subduction zones on plate dynamics. *Journal of Geophysical Research*, *104*, 17,551–17,571. https://doi.org/10.1029/1999JB900149

Davies, G. F. (1995). Penetration of plates and plumes through the mantle transition zone. *Earth and Planetary Science Letters*, *133*(3–4), 507–516. https://doi.org/10.1016/0012-821X(95)00039-F

Di Leo, J. F., Walker, A. M., Li, Z. H., Wookey, J., Ribe, N. M., Kendall, J. M., & Tommasi, A. (2014). Development of texture and seismic anisotropy during the onset of subduction. *Geochemistry, Geophysics, Geosystems*, *15*, 192–212. https://doi.org/10.1002/2013GC005032

Díaz, J., & Gallart, J. (2014). Seismic anisotropy from the Variscan core of Iberia to the Western African Craton: New constrains on upper mantle flow at regional scales. *Earth and Planetary Science Letters*, *394*(Supplement C), 48–57. https://doi.org/10.1016/j.epsl.2014.03.005

Díaz, J., Gallart, J., Morais, I., Silveira, G., Pedreira, D., Pulgar, J. A., et al. (2015). From the Bay of Biscay to the High Atlas: Completing the anisotropic characterization of the upper mantle beneath the westernmost Mediterranean region. *Tectonophysics*, *663*, 192–202. https://doi.org/10.1016/j.tecto.2015.03.007

Díaz, J., Gil, A., & Gallart, J. (2013). Uppermost mantle seismic velocity and anisotropy in the Euro-Mediterranean region from Pn and Sn tomography. *Geophysical Journal International*, *192*(1), 310–325. https://doi.org/10.1093/gji/ggs016

Duggen, S., Hoernle, K., van den Bogaard, P., & Garbe-Schönberg, D. (2005). Post-collisional transition from subduction to intraplate-type magmatism in the westernmost Mediterranean: Evidence for continental-edge delamination of subcontinental lithosphere. *Journal of Petrology*, *46*(6), 1155–1201. https://doi.org/10.1093/petrology/egi013

Faccenda, M., & Capitanio, F. A. (2013). Seismic anisotropy around subduction zones: Insights from three-dimensional modeling of upper mantle deformation and SKS splitting calculations. *Geochemistry, Geophysics, Geosystems*, *14*, 243–262. https://doi.org/10.1029/2012GC004451

Faccenna, C., Becker, T. W., Auer, L., Billi, A., Boschi, L., Brun, J. P., et al. (2014). Mantle dynamics in the Mediterranean. *Reviews of Geophysics*, *52*, 283–332. https://doi.org/10.1002/2013RG000444

Faccenna, C., Davy, P., Brun, J. P., Funiciello, R., Giardini, D., Mattei, M., & Nalpas, T. (1996). The dynamics of back-arc extension: An experimental approach to the opening of the Tyrrhenian Sea. *Geophysical Journal International*, *126*(3), 781–795. https://doi.org/10.1111/j.1365-246X.1996.tb04702.x

Faccenna, C., Piromallo, C., Crespo-Blanc, A., Jolivet, L., & Rossetti, F. (2004). Lateral slab deformation and the origin of the western Mediterranean arcs. *Tectonics*, *23*, TC1012. https://doi.org/10.1029/2002TC001488

Funiciello, F., Faccenna, C., & Giardini, D. (2004). Role of lateral mantle flow in the evolution of subduction systems: Insights from laboratory experiments. *Geophysical Journal International*, *157*(3), 1393–1406. https://doi.org/10.1111/j.1365-246X.2004.02313.x

Funiciello, F., Faccenna, C., Giardini, D., & Regenauer-Lieb, K. (2003). Dynamics of retreating slabs: 2. Insights from three-dimensional laboratory experiments. *Journal of Geophysical Research*, *108*(4), 2207. https://doi.org/10.1029/2001JB000896

Funiciello, F., Faccenna, C., Heuret, A., Lallemand, S., Di Giuseppe, E., & Becker, T. W. (2008). Trench migration, net rotation and slab–mantle coupling. *Earth and Planetary Science Letters*, *271*(1–4), 233–240. https://doi.org/10.1016/j.epsl.2008.04.006

Funiciello, F., Moroni, M., Piromallo, C., Faccenna, C., Cenedese, A., & Bui, H. A. (2006). Mapping mantle flow during retreating subduction: Laboratory models analyzed by feature tracking. *Journal of Geophysical Research*, *111*, B03402. https://doi.org/10.1029/2005JB003792

Garel, F., Goes, S., Davies, D. R., Davies, J. H., Kramer, S. C., & Wilson, C. R. (2014). Interaction of subducted slabs with the mantle transition-zone: A regime diagram from 2-D thermo-mechanical models with a mobile trench and an overriding plate. *Geochemistry, Geophysics, Geosystems*, *15*, 1739–1765. https://doi.org/10.1002/2014GC005257

Griffiths, R. W., Hackney, R. I., & van der Hilst, R. D. (1995). A laboratory investigation of effects of trench migration on the descent of subducted slabs. *Earth and Planetary Science Letters*, *133*(1–2), 1–17. https://doi.org/10.1016/0012-821X(95)00027-A

Guillou-Frottier, L., Buttles, J., & Olson, P. (1995). Laboratory experiments on the structure of subducted lithosphere. *Earth and Planetary Science Letters*, *133*(1–2), 19–34. https://doi.org/10.1016/0012-821X(95)00045-E

Hall, R., & Spakman, W. (2015). Mantle structure and tectonic history of SE Asia. *Tectonophysics*, *658*(25), 14–45. https://doi.org/10.1016/j.tecto.2015.07.003

Handy, M. R., Ustaszewski, K., & Kissling, E. (2014). Reconstructing the Alps-Carpathians-Dinarides as a key to undertanding switches in subduction polarity, slab gaps and surface motion. *International Journal of Earth Sciences*, *104*(1), 1–26. https://doi.org/10.1007/s00531-014-1060-3

van Hinsbergen, D. J. J., Vissers, R. L. M., & Spakman, W. (2014). Origin and consequences of western Mediterranean subduction, rollback, and slab segmentation. *Tectonics*, *33*, 393–419. https://doi.org/10.1002/tect.20125

Holt, A. F., Royden, L. H., & Becker, T. W. (2017). The dynamics of double slab subduction. *Geophysical Journal International*, *209*, 250–265.

King, P. B. (2000). Tectonic reconstructions of New Zealand: 40 Ma to the Present. *New Zealand Journal of Geology and Geophysics*, *43*(4), 611–638. https://doi.org/10.1080/00288306.2000.9514913

Király, Á., Capitanio, F. A., Funiciello, F., & Faccenna, C. (2016). Subduction zone interaction: Controls on arcuate belts. *Geology*, *44*(9), 715–718. https://doi.org/10.1130/G37912.1

Király, Á., Capitanio, F. A., Funiciello, F., & Faccenna, C. (2017). Subduction induced mantle flow: Length-scales and orientation of the toroidal cell. *Earth and Planetary Science Letters*, *479*, 284–297. https://doi.org/10.1016/j.epsl.2017.09.017

Kufner, S.-K., Schurr, B., Sippl, C., Yuan, X., Ratschbacher, L., Akbar, A., et al. (2016). Deep India meets deep Asia: Lithospheric indentation, delamination and break-off under Pamir and Hindu Kush (Central Asia). *Earth and Planetary Science Letters*, *435*, 171–184. https://doi.org/10.1016/j.epsl.2015.11.046

Lallemand, S., Font, Y., Bijwaard, H., & Kao, H. (2001). New insights on 3-D plates interaction near Taiwan from tomography and tectonic implications. *Tectonophysics*, *335*(3–4), 229–253. https://doi.org/10.1016/S0040-1951(01)00071-3

Lallemand, S., Heuret, A., Faccenna, C., & Funiciello, F. (2008). Subduction dynamics as revealed by trench migration. *Tectonics*, *27*, TC3014. https://doi.org/10.1029/2007TC002212

Lamb, S. (2011). Cenozoic tectonic evolution of the New Zealand plate-boundary zone: A paleomagnetic perspective. *Tectonophysics*, *509*(3–4), 135–164. https://doi.org/10.1016/j.tecto.2011.06.005

Li, Z. H., & Ribe, N. M. (2012). Dynamics of free subduction from 3-D boundary element modeling. *Journal of Geophysical Research*, *117*, B06408. https://doi.org/10.1029/2012JB009165

Liao, J., Gerya, T., Thielmann, M., Webb, A., Kufner, S.-K., & Yin, A. (2017). 3D geodynamic models for the development of opposing continental subduction zones: The Hindu Kush-Pamir example. *Earth and Planetary Science Letters*, *480*, 133–146. https://doi.org/10.1016/j.epsl.2017.10.005

Lin, S.-C., & Kuo, B.-Y. (2016). Dynamics of the opposite-verging subduction zones in the Taiwan region: Insights from numerical models. *Journal of Geophysical Research: Solid Earth*, *121*, 2174–2192. https://doi.org/10.1002/2015JB012784

Long, M. D. (2016). The Cascadia Paradox: Mantle flow and slab fragmentation in the Cascadia subduction system. *Journal of Geodynamics*, *102*, 151–170. https://doi.org/10.1016/j.jog.2016.09.006

Long, M. D., & Silver, P. G. (2008). The subduction zone flow field from seismic anisotropy: A global view. *Science*, *319*(5861), 315–318. https://doi.org/10.1126/science.1150809

Lustrino, M., & Wilson, M. (2007). The circum-Mediterranean Anorogenic Cenozoic igneous province. *Earth-Science Reviews*, *81*, 1–65.

Lustrino, M., Duggen, S., & Rosenberg, C. L. (2011). The central-western Mediterranean: anomalous igneous activity in an anomalous collisional tectonic setting. *Earth-Science Reviews*, *104*, 1–40.

Magni, V., Faccenna, C., Van Hunen, J., & Funiciello, F. (2013). Delamination vs. break-off: The fate of continental collision. *Geophysical Research Letters*, *40*, 285–289. https://doi.org/10.1002/grl.50090

Melchiorre, M., Vergés, J., Fernàndez, M., Coltorti, M., Torne, M., & Casciello, E. (2017). Evidence for mantle heterogeneities in the westernmost Mediterranean from a statistical approach to volcanic petrology. *Lithos*, *276*, 62–74. https://doi.org/10.1016/j.lithos.2016.11.018

Meyer, C., & Schellart, W. P. (2013). Three-dimensional dynamic models of subducting plate-overriding plate-upper mantle interaction. *Journal of Geophysical Research: Solid Earth*, *118*, 775–790. https://doi.org/10.1002/jgrb.50078

Mishin, Y. A., Gerya, T. V., Burg, J. P., & Connolly, J. A. D. (2008). Dynamics of double subduction: Numerical modeling. *Physics of the Earth and Planetary Interiors*, *171*(1–4), 280–295. https://doi.org/10.1016/j.pepi.2008.06.012

Moresi, L., Betts, P. G., Miller, M. S., & Cayley, R. A. (2014). Dynamics of continental accretion. *Nature*, *508*(7495), 245–248. https://doi.org/10.1038/nature13033

Morra, G., Chatelain, P., Tackley, P., & Koumoutsakos, P. (2009). Earth curvature effects on subduction morphology: Modeling subduction in a spherical setting. *Acta Geotechnica*, *4*(2), 95–105. https://doi.org/10.1007/s11440-008-0060-5

Morra, G., Regenauer-Lieb, K., & Giardini, D. (2006). Curvature of oceanic arcs. *Geology*, *34*(10), 877–880. https://doi.org/10.1130/G22462.1

Mullen, E. K., & Weis, D. (2015). Evidence for trench-parallel mantle flow in the northern Cascade Arc from basalt geochemistry. *Earth and Planetary Science Letters*, *414*, 100–107. https://doi.org/10.1016/j.epsl.2015.01.010

Palano, M., Piromallo, C., & Chiarabba, C. (2017). Surface imprint of toroidal flow at retreating slab edges: The first geodetic evidence in the Calabrian subduction system. *Geophysical Research Letters*, *44*, 845–853. https://doi.org/10.1002/2016GL071452

Ribe, N. M. (2010). Bending mechanics and mode selection in free subduction: A thin-sheet analysis. *Geophysical Journal International*, *180*(2), 559–576. https://doi.org/10.1111/j.1365-246X.2009.04460.x

Schellart, W. P. (2004). Kinematics of subduction and subduction-induced flow in the upper mantle. *Journal of Geophysical Research*, *109*, B07401. https://doi.org/10.1029/2004JB002970

Schellart, W. P. (2008). Kinematics and flow patterns in deep mantle and upper mantle subduction models: Influence of the mantle depth and slab to mantle viscosity ratio. *Geochemistry, Geophysics, Geosystems*, *9*, Q03014. https://doi.org/10.1029/2007GC001656

Schellart, W. P. (2010). Evolution of subduction zone curvature and its dependence on the trench velocity and the slab to upper mantle viscosity ratio. *Journal of Geophysical Research*, *115*, B11406. https://doi.org/10.1029/2009JB006643

Schellart, W. P., & Moresi, L. (2013). A new driving mechanism for backarc extension and backarc shortening through slab sinking induced toroidal and poloidal mantle flow: Results from dynamic subduction models with an overriding plate. *Journal of Geophysical Research: Solid Earth*, *118*, 3221–3248. https://doi.org/10.1002/jgrb.50173

Spakman, W., & Wortel, R. (2004). A tomographic view on Western Mediterranean geodynamics. In W. Cavazza, F. Roure, W. Spakman, G. M. Stampfli, & P. Ziegler (Eds.), *The TRANSMED Atlas, The Mediterranean Region from Crust to Mantle* (pp. 31–52). Berlin, Heidelberg: Springer. https://doi.org/10.1007/978-3-642-18919-7_2

Stegman, D. R., Farrington, R., Capitanio, F. A., & Schellart, W. P. (2010). A regime diagram for subduction styles from 3-D numerical models of free subduction. *Tectonophysics*, *483*(1–2), 29–45. https://doi.org/10.1016/j.tecto.2009.08.041

Stegman, D. R., Freeman, J., Schellart, W. P., Moresi, L., & May, D. (2006). Influence of trench width on subduction hinge retreat rates in 3-D models of slab rollback. *Geochemistry, Geophysics, Geosystems*, *7*, Q03012. https://doi.org/10.1029/2005GC001056

Strak, V., & Schellart, W. P. (2014). Evolution of 3-D subduction-induced mantle flow around lateral slab edges in analogue models of free subduction analysed by stereoscopic particle image velocimetry technique. *Earth and Planetary Science Letters*, *403*, 368–379. https://doi.org/10.1016/j.epsl.2014.07.007

Ten Grotenhuis, S. M., Piazolo, S., Pakula, T., Passchier, C. W., & Bons, P. D. (2002). Are polymers suitable rock analogs? *Tectonophysics*, *350*(1), 35–47. https://doi.org/10.1016/S0040-1951(02)00080-X

Thielicke, W., & Stamhuis, E. J. (2014). PIVlab – Towards user-friendly, affordable and accurate digital particle image velocimetry in MATLAB. *Journal of Open Research Software*, *2*(1), e30. https://doi.org/10.5334/jors.bl

Vergés, J., & Fernàndez, M. (2012). Tethys-Atlantic interaction along the Iberia-Africa plate boundary: The Betic-Rif orogenic system. *Tectonophysics*, *579*, 144–172. https://doi.org/10.1016/j.tecto.2012.08.032

Vignaroli, G., Faccenna, C., Jolivet, L., Piromallo, C., & Rossetti, F. (2008). Subduction polarity reversal at the junction between the Western Alps and the Northern Apennines, Italy. *Tectonophysics*, *450*(1–4), 34–50. https://doi.org/10.1016/j.tecto.2007.12.012

Wallace, L. M., Ellis, S., & Mann, P. (2009). Collisional model for rapid fore-arc block rotations, arc curvature, and episodic back-arc rifting in subduction settings. *Geochemistry, Geophysics, Geosystems*, *10*, Q05001. https://doi.org/10.1029/2008GC002220

Wallace, L. M., Stevens, C., Silver, E., McCaffrey, R., Loratung, W., Hasiata, S., et al. (2004). GPS and seismological constraints on active tectonics and arc-continent collision in Papua New Guinea: Implications for mechanics of microplate rotations in a plate boundary zone. *Journal of Geophysical Research*, *109*, B05404. https://doi.org/10.1029/2003JB002481

Weijermars, R. (1986). Flow behaviour and physical chemistry of bouncing putties and related polymers in view of tectonic laboratory applications. *Tectonophysics*, *124*(3–4), 325–358. https://doi.org/10.1016/0040-1951(86)90208-8

Weijermars, R., & Schmeling, H. (1986). Scaling of Newtonian and non-Newtonianfluid dynamics without inertia for quantitative modelling of rock flow due togravity (including the concept of rheological similarity). *Physics of the Earth and Planetary Interiors*, *43*(4), 316–330. https://doi.org/10.1016/0031-9201(86)90021-X

Wortel, R. (1982). Seismicity and rheology of subducted slabs. *Nature*, *296*(5857), 553–556. https://doi.org/10.1038/296553a0

Yamato, P., Husson, L., Braun, J., Loiselet, C., & Thieulot, C. (2009). Influence of surrounding plates on 3D subduction dynamics. *Geophysical Research Letters*, *36*, L07303. https://doi.org/10.1029/2008GL036942

Zhu, H., & Tromp, J. (2013). Mapping tectonic deformation in the crust and upper mantle beneath Europe and the North Atlantic Ocean. *Science*, *341*(6148), 871–875. https://doi.org/10.1126/science.1241335